RSC Advances

This is an *Accepted Manuscript*, which has been through the Royal Society of Chemistry peer review process and has been accepted for publication.

Accepted Manuscripts are published online shortly after acceptance, before technical editing, formatting and proof reading. Using this free service, authors can make their results available to the community, in citable form, before we publish the edited article. This *Accepted Manuscript* will be replaced by the edited, formatted and paginated article as soon as this is available.

You can find more information about *Accepted Manuscripts* in the Information for Authors.

Please note that technical editing may introduce minor changes to the text and/or graphics, which may alter content. The journal's standard Terms & Conditions and the Ethical guidelines still apply. In no event shall the Royal Society of Chemistry be held responsible for any errors or omissions in this *Accepted Manuscript* or any consequences arising from the use of any information it contains.

ROYAL SOCIETY OF CHEMISTRY

www.rsc.org/advances

Preparation of metallic pivot-based imprinted monolith with hydrophilic macromonomer

Xiu-Yuan Li [a,b] Li Ma[a,b] Yan-Ping Huang [a,b] Zhao-Sheng Liu*, [a,b] Haji Akber Aisa [*, a,b]

[a]*Key Laboratory of Plant Resources and Chemistry of Arid Zone, Xinjiang Technical Institute of Physics and Chemistry, Chinese Academy of Sciences, 40-1 South Beijing Road, Urumqi 830011, Xinjiang, China*

[b]*State Key Laboratory Basis of Xinjiang Indigenous Medicinal Plants Resource Utilization, Xinjiang Technical Institute of Physics and Chemistry, Chinese Academy of Sciences, Urumqi 830011,China*

Correspondence: Dr. Zhao-Sheng Liu

Fax: (+086)-022-23536746

E-mail: zhaoshengliu@sohu.com

Correspondence: Haji Akber Aisa

E-mail: haji@ms.xjb.ac.cn

Keywords: Monolith; molecularly imprinted polymer; metallic pivot; molecular recognition; hydrophilic monomer; affinity

RSC Advances Accepted Manuscript

27

RSC Advances Accepted Manuscript

Abstract

A new metallic pivot-based molecularly imprinted polymer (MIPs) was developed to enhance imprinting effect of water-soluble template. Hydrophilic macromonomer oligo(ethyleneglycol) methyl ether methacrylate (OEG), bearing a small oligoethylene glycol side chain, was introduced into MIPs matrix in order to achieve good selectivity and lower hydrophobic characterization. In a ternary porogenic system of dimethyl sulfoxide -dimethylformamide-1-butyl-3-methylimidazolium tetrafluoroborate, an imprinted monolithic column with high porosity and good permeability was synthesized using a mixture of gallic acid (template), 4-vinylpyridine (4-VP), ethylene glycol dimethacrylate, and nickel acetate. Some polymerization variables, such as ratio of OEG/4-VP and ratio of template to nickel ions, on the imprinting effect of the resulting MIPs monoliths were systematically investigated. The greatest imprinting factor of 8.63 was achieved on the water compatibility MIPs monolith with the optimized polymerization parameters. In addition, Freundlich analyses indicated that Ni^{2+} mediated OEG MIP had homogeneous affinity with heterogeneity index of 0.87 compared with Ni^{2+} mediated OEG-free MIP (0.65) and Ni^{2+}-free OEG MIP (0.67).

RSC Advances Accepted Manuscript

Introduction

Molecularly imprinted polymers (MIPs) have been proved to be a synthetic material with highly specific molecular recognition ability.[1, 2] The preparation of MIPs involves using a target molecule as template, which directs the self-assembly of functional monomers that are subsequently co-polymerized in the presence of cross-linking monomers. With tailored selectivity, easy preparation, and chemical robustness, MIPs can be employed as specific affinity matrix for the target template. Impressive progress has been made over the past few years in the production of materials for various analytical and separation applications[3, 4] due to a better understanding of the mechanisms of forming imprints. Recent developments in the use of MIPs for chromatographic stationary phases,[5-7] solid-phase extraction, [8,9] drug release,[10,11] catalysis,[12,13] and biosensing[14-16] have been reported.

Preparing MIPs for polar compounds such as water-soluble phenolic acid is much more difficult than non-polar template. Optimally, preparative conditions are the same as re-binding conditions because the same compositions of both preparative and re-binding media can favor the recognition to the template.[17] Concerning this matter, the preparation of MIPs for water-soluble template in aqueous solution is better than in organic solution. However, the protocol of MIP preparation for organic compounds has generally been based on hydrogen bonding interactions in non-polar solvents, which is weakened in aqueous solution due to the competition of water. Furthermore, non-selective adsorption is often observed on the conventional MIP, originating from hydrophobic interactions on the surface of the polymer matrix.[17]

RSC Advances Accepted Manuscript

Consequently, a novel method of preparing the MIPs containing hydrophilic units is needed.

The use of a highly aqueous solvated cross-linker such as pentaerythritol triacrylate[18] or N, N-methylenebisacrylamide[19] to prepare hydrophilic MIPs is a choice to solve the problems above. Nevertheless, the interactions between these hydrophilic cross-linkers and solvent in rebinding procedure may cause the deformation of imprinting cavities or even collapses between functional monomer and template, and this worsens the recognition properties of MIPs. Recently, a new synthetic strategy of copolymerization of the functional monomer with a macromonomer has been developed.[20] The hydrophilic monomer bears a small oligoethylene glycol side chain and can increase the hydrophilicity of imprinted cavities while maintaining a conventional concentration of the usual cross-linkers. However, the introduction of macromonomer segments caused a decrease in the capacity factors of the polymers since the analytes are less retained by nonspecific hydrophobic interactions and pass through the polymer network faster due to increased hydrophilicity by such segments. Consequently, a novel method of preparing the hydrophilic MIPs that has higher retention and affinity is desired.

For the MIPs created by noncovalent imprinting, monomers that can undergo noncovalent interactions are brought together with the template molecule and monomer to form well-defined complexes. Thus, the achievable selectivity of the resultant MIPs is governed by the nature and stability of these complexes. Generally applicable approach for stabilizing the complex is to design a particular functional monomer capable of forming strong interactions with template. For example, the

RSC Advances Accepted Manuscript

functional monomer forming strong pre-polymerization complexes with the template in a stoichiometric ratio,[21,22] can generate imprinted polymers with binding sites of higher affinity and increasing retention. In addition, a number of works have demonstrated that the interactions between the template molecule and functional monomers could be stabilized by macromolecular crowding agent to increase the retention of MIPs.[23-25]

Use of a metallic pivot for self-assembly has revealed to produce highly specific MIPs effectively.[26-29] Using this strategy, the weak linkage between the monomer and template, such as hydrogen bond or Coulomb force, is replaced by stronger coordination binding. This stabilization originated from metal ion-mediated self-organized architecture leads to a decrease of thermal and mechanical motions of monomers or oligomer-template. Assembling with metal ion as the pivot, in other words, monomers are regularly positioned around the template via coordinative bridge, which largely restrains the relative motion of monomers or oligomer-template. As a result, the relatively higher fidelity of imprint can be achieved by this approach.

In view of the facts above, it is intriguing for us to investigate whether assembling with metal ion as the pivot can be utilized to prepare hydrophilic MIPs with enhanced affinity. In this work, we prepared OEG-based imprinted monolith with nickel ions as pivot for the first time. Monolithic format of MIPs is desired because the general problems of MIPs preparation using conventional bulk polymerization can be avoided [5]. Gallic acid (GA) was selected as model water-soluble template and 4-vinylpyridine (4-VP) as functional monomer. The effect of polymerization parameters such as the ratio of OEG/4-VP and ratio of the template to nickel ions on the imprinting effect of this new MIP monolith was investigated. Binding

RSC Advances Accepted Manuscript

characteristic and homogeneity of the imprinting sites on the metal ion-mediated OEG MIP were studied in detail. Furthermore, the selectivity of the novel MIP was evualated by comparing retention properties of structural analogues of GA (Fig. 1) on the Ni^{2+}-mediated OEG MIP, Ni^{2+}-mediated OEG-free MIP and Ni^{2+}-free OEG MIP.

Results and discussion

Preparation of metallic pivot-based OEG imprinted monolith

This work is an efford to improve imprinting effect of MIP with good water compatibility. The enhanced molecular recognition towards the imprint species is expected to be achieved by reducing nonspecific hydrophobic interaction using hydrophilic macromonomer based on a strategy of metallic pivot. To investigate the effect of assembling with metal ion as the pivot to enhance affinity of the resulting hydrophilic MIPs, we prepared the OEG-based MIPs in a monolithic format (Table 1). In present work, porogen formulation is crucial to prepare metallic pivot-based imprinted monolith with hydrophilic macromonomer. On the one hand, the porogenic solvent can solve polar template molecule, hydrophilic OEG and metal ion. Next, the porogen should produce large pores to assure good flow-through properties of the resultant MIP. On the other hand, the porogenic solvent should avoid the disturbance caused by polar solvent during the polymerization in addition to its influence on the polymer morphology. It was found that previously developed porogenic system, [30] a ternary mixture of DMSO, DMF and $[BMIM]BF_4$ can solve the problems above (Table 1). $[BMIM]BF_4$ was found a unique IL to afford good permeability for the resulting monolithic MIP. Other imidazolium-based IL with varying cation alkyl

RSC Advances Accepted Manuscript

chain length (C4–C16) containing same anion (BF_4^-) led to MIP monoliths with very high back pressure thus can not be evaluated further. Anion type ionic liquids in fixed imidazolium cations ($[BMIM]^+$) was also used to be the composition of porogenic solvent. Miscibility of the cation type of ionic liquid ($[BMIM]PF_6$ or $[BMIM]HSO_4$) with pre-polymerization mixture limited the use in this study.

In the first attempt to prepare GA-imprinted monolith in the presence of OEG, MIP monolith C5 was made in the absence of metal ion. The resulting MIP did not show any recognition ability, maybe due to the high polarity of the solvent used in the polymerization system (DMSO, DMF and $[BMIM]BF_4$)[30] affecting the formation of the template–monomer complex. The interaction between the functional monomer and template in non-covalent MIP may include hydrogen bond, hydrophobic, charge transfer, or other forms. However, the formation of template–monomer complex in polar solvent cannot be efficient enough, because the hydrogen bonding interaction between GA and monomers can be interrupted by polar solvent. In order to avoid the disturbance caused by polar solvent during the polymerization, metal ions as mediator had been introduced during the pre-polymerization to form the stronger complex of template–metal ion–monomer.[26-29] In the present study, greater imprinting effect (IF = 8.63) was obtained on the Ni^{2+}-mediated OEG MIPs (C11) (Fig. 2). Selectivity factors (α) of GA on MIP C11 for its analogues were all increased in comparison with the corresponding NIP. As shown in Fig. 3, higher IF showed that Ni^{2+} played a vital role in the formation of the MIP materials. Retention factor of the MIP without metal ions involved was almost the same as that of the NIP. In other words, IF value of the MIP

RSC Advances Accepted Manuscript

was closed to 1, showing little imprinting effect. In this case, assembling with metal as pivot, the monomer and the template are bridged through coordination bond. This effect might owe to that a more stable ternary complex of monomer–metal ions–template can be formed in polar solvents before polymerization, in which GA and 4-VP could strongly chelate with Ni^{2+} through carboxyl groups and pyridine groups, respectively. Thus, the crucial role of metal ion to achieve a complete self-assembly for an effective imprinting was demonstrated to the polar template in the polar porogen.

The morphology of the Ni^{2+}-mediated OEG MIP, Ni^{2+}-free OEG MIP and Ni^{2+}-mediated OEG-free MIP was observed by SEM (Fig. 4). An agglomerate of microspheres with a coarse surface that were fused into a continuous structure and the typical bimodal pore-size distribution (4-6 μm macropores) was visible on the Ni^{2+}-mediated OEG MIP. In contrast, on the textures of the Ni^{2+}-mediated OEG-free MIP, microglobules of relatively uniform size were agglomerated to larger clusters and greater sizes were observed. In addition, the micrograph of the Ni^{2+}-free OEG MIP showed microglobules of smaller size. The results indicated that the existence of the template or Ni^{2+} would have remarkable influence on the size of the microglobules.

To ensure that the superior retention observed at the selected MIPs is not simply a surface effect, multipoint BET measurement for the three MIPs was performed to get pore characterization. As shown in Fig. 5a, all the monoliths display “type IV” isotherms which are usually related to meso-macroporous materials.[31] The hysteresis

RSC Advances Accepted Manuscript

loops resemble H3 types with desorption branch leading to closure point at P/P_0 value of non-zero, suggesting the specific structure of slit-shapes pores. BET surface area of the OEG MIP C11 calculated from the adsorption data was 13.41 m^2/g. In addition, a maximum corresponding to pore diameter of about 26.55 nm was observed for the OEG MIP in desorption-based distribution curve (Fig. 5b), indicating smaller mesopores than the other MIP monoliths.[30, 32] BET surface area of the conresponding MIP without OEG or Ni^{2+} was 10.69 m^2/g and 28.32 m^2/g, respectively. Apparently, the presence of the OEG or Ni^{2+} has little effect on the pore structure of the resulting MIP monolith. Thus, the contribution of pore structure and morphology to the imprinting effect of the OEG-based MIP was minor compared with the interaction between functional monomer, metallic pivot and the template. This result precludes the assumption that the highest retention during chromatographic separation is merely a consequence of increased overall surface area. Therefore, further investigation is required to establish precisely how the pre-organization of monomer-template-metal ion affects the progression of a polymerization and leads to differences in the imprinting factors.

Effect of polymerization variables on molecular recognition

Effect of OEG/4-VP molar ratio

Considering that conventional polymerization parameters to metallic pivot-based MIPs have been investigated in detail previously,[27,29] we focused on three polymerization variables related to the OEG-based MIP in present study. One of the variables is the molar ratio of OEG/4-VP in the polymerization mixture. It seemed

RSC Advances Accepted Manuscript

that the interaction between OEG and the template was not involved in the recognition of the resulting MIP. To examine this assumption, an NMR study was conducted with a pseudo-pre-polymerization mixture consisting of OEG, 4-VP, and GA. The initiator AIBN was omitted because of its insignificant involvement in complex formation. The crosslinker EDMA was also omitted because its carbonyl group could not be involved in hydrogen bonding with the template, avoiding the system too complicated to observe the complexation between 4-VP or OEG and the template. The concentrations of 4-VP and the template were as the same as those used in the polymerization. As shown in Fig. S1, with the addition of OEG to GA solution, the peak derived from a carboxyl proton of GA was not shifted downfield, suggesting the no formation of hydrogen bonds between GA and OEG.

To achieve the optimized result of imprinting, the stoichiometric ratio of OEG/4-VP for the MIP preparation studied was set at 2.5:1, 2:1, 1.5:1 and 1:1, respectively (Table S1). When low level of 4-VP was used, the undesirable effect of imprinting was observed. This may be attributed to a relative excess of the template, which leads to the loss of site integrity due to coalescence of binding sites derived from the template self-association.[33] The maximum imprinting factor was observed at OEG/4-VP ratio of 2:1 (Fig. 6).

Effect of the molar ratio of cross-linking monomer to functional monomer

For the non-covalent approach, the relationship between the cross-linking degree of the polymers and its recognition property is rather complicated. In a few cases, high levels of crosslinker caused an increase in selectivity of the resulting MIPs.[34] In

RSC Advances Accepted Manuscript

another case, it was observed that the selectivity reached to a maximum at one lower degree of cross-linking.[35] In present work, it was observed that high levels of crosslinker resulted in a notable decrease of imprinting factor from 8.63 to 1.16 (Fig. 7). This may be explained by the severely increased stiffness of the polymer network, thus decreased accessibility of the cavities significantly.[1] The optimal degree of crosslinking was found to be 65% in terms of imprinting factor, which is lower than conventional 80%. Possible reason is the balance of site stability, integrity and accessibility at the level of intermediate level of crosslinker due to the pre-organization of GA-Ni^{2+}-4-VP complex in the preparation of MIPs monolith.

Effect of the molar ratio of template to nickel ions

It should be noted that not all the OEG-based MIPs with Ni^{2+} participation have larger IFs. It can be inferred from the results of Table S2 that other factors such as the species of functional monomers and template molecules also exert impact on molecular imprinting effect of the MIP. To study the effect from the mediation of nickel ions to the interaction between GA to 4-VP, we prepared a number of Ni^{2+}-mediated MIP monoliths by setting the ratio of GA to 4-VP of 1:6 and 4-VP to EDMA of 1:4. The retention behaviors of the template molecule on the nickel ion-mediated MIP monolith were evaluated by using a mobile phase of acetonitrile/acetate buffer (pH 3.6) (90/10, v/v). As shown in Table S2, when the molar ratio of Ni^{2+} to GA decreased from 1:1 to 1:2, the retention factor of GA on the imprinted monolith was decreased from 1.96 to 0.60. Corresponding IF value shifted from 11.53 to 0.34. In contrast, when no nickel ions was used, the retention factor of

RSC Advances Accepted Manuscript

GA on the MIP (k = 4.16) and NIP (k = 4.39) did not vary much with IF value of 0.95. Apparently, a non-stoichiometric ratio of Ni^{2+} to GA adversely affects the specific binding, maybe due to a decrease in the amount of imprinting complex of 4-VP-Ni^{2+}-GA at other ratio. The stoichiometric ratio-dependent phenomena indicated that for the ion-mediated imprinting system here there are interactions existing bilaterally in the monomer-template, monomer-metal and template-metal, which are subsequently saturated by setting a stoichiometric amount of monomer and template.

Recognition mechanism of imprinted monolith

pH effect of mobile phase on retention property

The rebinding of GA to the Ni^{2+}-mediated OEG MIP is strongly dependent on the mobile phase used. In this study, acetonitrile/ acetate buffer (70/30, v/v) with a range of pH from 3.0 to 7.0 was used as mobile phase to evaluate pH effect on imprinting factors. The pH impact on the recognition of the template is shown in Fig. 8 and binding on the Ni^{2+}-mediated OEG MIP (C11) is strongly influenced by electrostatic interactions. The maximum imprinting factor (above 10) was observed at an eluent pH of 5.0, a value close to the pK_a (= 5.3) of GA. At one pH unit above the pK_a value, a certain percentage of the molecule will be deprotonated (negatively charged). As the pH nears the pK_a value, the amount of molecules negatively charged decreases (it will be 50% at the pK_a value). Thus, this indicates that the retention is controlled by an ion-exchange process.[36] Further increase of pH in mobile phase led to a peak split of GA and the measurement of retention factor thus imprinting factor was impossible. It should be noted that similar retention factors of GA can be observed on all three NIP

RSC Advances Accepted Manuscript

but the retention on Ni^{2+}-mediated OEG-free MIP (C15) or Ni^{2+}-free OEG MIP (C5) was totally different form the Ni^{2+}-mediated OEG MIP (C11). In addition, the analogs of GA showed varying retention behaviors on Ni^{2+}-mediated OEG-free MIP (C15) or Ni^{2+}-free OEG MIP (C5) except MG (Fig. S2 and S3).

Influence of organic phase composition on retention property

The influence of organic modifier in a mixture of acetonitrile-acetate buffer on the retention factor of GA and its analogues were studied using the Ni^{2+}-mediated OEG MIP (C11) and non-imprinted monolith (C12). A mixture of acetonitrile-acetate buffer solution (50 mmol L^{-1}, pH 3.6) was used as the mobile phase, with the content of acetonitrile ranging from 20% to 90%. As shown in Fig. 9, the retention factors of the template decreased with decreasing acetonitrile amount from 90% to 50%. While the amount of acetonitrile decreased from 50% to 20% the retention factors increased. These results implied a change in the retention mode from a an electrostatically driven mode in water-poor system to the desolvation retention at higher water contents on the Ni^{2+}-based imprinted column.[37] In contrast, similar retention behaviors can not be observed on the Ni^{2+}-mediated OEG-free MIP (C15) and Ni^{2+}-free OEG MIP (C5) in spite of same trend in retention on all three NIP. It should be noted that MG is a molecule strictly resembling the template, characterized by the sole absence of a methyl. As shown in Fig. 9, a greater difference in retention properties for the template was observed on the ion-mediated OEG MIP, the Ni^{2+}-mediated OEG-free MIP and Ni^{2+}-free OEG MIP, which showed good selectivity of the GA-imprinted polymer. Furthermore, the tested structural analogues, such as SA, MHA, PHA, EA

RSC Advances Accepted Manuscript

and DHA, had shown different retention properties on the Ni^{2+}-mediated OEG-free MIP (C15) or Ni^{2+}-free OEG MIP (C5) (Fig. S4 and S5).

Binding characteristic of MIP monolith

The binding characteristic between the template and the imprinted polymer can be determined by frontal chromatography (data not shown). Affinity of the imprinted polymers was determined by Scatchard-Rosenthal analysis (Fig. S6) and nonlinear profiles were observed. The assessment was therefore conducted, paying particular attention to a partially linear section observed at a range of 1-12 μM where relatively high-affinity binding sites of each polymer can be estimated. The dissociation constant K_d of the Ni^{2+} mediated OEG MIP (C11), the Ni^{2+} mediated OEG-free MIP (C15) and the Ni^{2+}-free OEG MIP (C5) was 9.26×10^{-4}, 5.49×10^{-3}, and 1.24×10^{-3} mol g^{-1}, respectively (Table 2). Noteworthy improvement of affinity of the MIP was also marked by the use of OEG, compared to the imprinting system using Ni^{2+} only. The enhanced imprinting effect may be attributed to decreased nonsepecific hydrophobic interactions since hydrophile segments of OEG can result in increased hydrophilicity thus less retention of analytes.[20] In addition, the result is suggestive for the improved accessibility of the imprinted cavities the fact that crosslinking desity is decreased by introducing OEG segment onto the matrix of the MIP. This can further be supported by comparing the number of binding sites between the OEG MIP (C11) and OEG-free MIP (C15). The corresponding number of selective binding sites of the Ni^{2+} mediated OEG MIP, the Ni^{2+} mediated OEG-free MIP and the Ni^{2+}-free OEG MIP was 32.2, 50.8, and 64.8 μmol g^{-1}, respectively. This meant that the number of binding sites of

RSC Advances Accepted Manuscript

high affinity at the Ni^{2+} mediated OEG MIP was about 2 times less than that at the Ni^{2+}-free OEG MIP. In addition, the number of non-selectivity binding sites at the former was about 2 times less than that at the latter. This leads us to a conclusion that Ni^{2+} plays a crucial role to increase the specificity and reduce the amount of non-selectivity sites.

To describe the surface heterogeneity for the adsorption process, Freundlich isotherm is often used to analyze the data of adsorption on MIPs.[38] The equation is frequently used in a linear from as

$$\lg Q_e = n \lg C_e + \lg K_f \qquad (1)$$

where C_e is the equilibrium concentration (mmol/L), Q_e the amount of GA adsorbed at the equilibrium (mmol/L), K_f isotherm constant (mmol/L), and n heterogeneity index. In most cases, the imprinted polymer has a higher degree of heterogeneity, i.e., a lower heterogeneity index, n, than its corresponding non-imprinted control.[38] In our study, the heterogeneities of the imprinted polymers were compared by fitting constants of K_f and n of the MIPs with the linear form of Eq. 1 (Fig. 109). The results showed that the Ni^{2+} mediated OEG MIP had a higher heterogeneity index (n = 0.87), suggesting the affinity sites of the MIP are more homogeneous. In contrast, the Ni^{2+} mediated OEG-free MIP and the Ni^{2+}-free OEG MIP showed lower heterogeneity index with heterogeneity index of 0.65 and 0.67, respectively.

Conclusions

A new strategy of combining metallic pivot and hydrophilic macromonomer was successfully developed to prepared GA-imprinted monolith. The greatest molecular

RSC Advances Accepted Manuscript

recognition ability towards the imprint species can be achieved at a molar ratio of OEG to 4-VP of 2:1 with good water compatibility. It was demonstrated that the affinity of the resulting MIP is a function of the molar ratio of metal ion to GA. The study of binding characteristic of the OEG MIP monolith showed that the number of affinity sites can be significantly shifted as the introduction of metal ion. Moreover, higher heterogeneity index indicated that the affinity sites of the metal ion-mediated OEG MIP monolith were more homogeneous. As a conclusion, the approach presented here may be an effective method to prepare MIP for water-soluble template with both good selectivity and lower hydrophobic characterization.

Experimental

Reagents and chemicals

Gallic acid (GA), salicylic acid (SA), *m*-hydroxybenzoic acid (MHA), and *p*-hydroxybenzoic acid (PHA), were obtained from Shanghai Guangtuo Chemical Reagent (Shanghai, China). Methyl gallate (MG) was from Beijing Bailingwei Chemical Reagent (Beijng, China). 4-Vinylpyridine (4-VP), ethylene glycol dimethacrylate (EDMA) and oligo(ethyleneglycol) methyl ether methacrylate (M_n = 300 $gmol^{-1}$, mean degree of polymerization 4-5) (OEG) were purchased from Sigma (St. Louis, MO, USA). Dimethyl sulfoxide (DMSO) and dimethylformamide (DMF) were obtained from Tianjin Jiangtian Chemical Industry Reagent (Tianjin, China). 1-Butyl-3-methylimidazolium tetrafluoroborate ([BMIM]BF_4) was purchased from Shanghai Chengjie Chemical Reagent (Shanghai, China). Nickel acetate and 2, 2-azobisisobutyronitrile (AIBN) were supplied by Kermel Chemical Reagent (Tianjin,

RSC Advances Accepted Manuscript

China). HPLC-grade acetonitrile (ACN) was from Tianjin Biaoshiqi Chemical Reagent (Tianjin, China). Other analytical reagents were from Tianjin Chemical Reagent Ltd. Co. (Tianjin, China).

Preparation of MIP monolithic columns

The preparation of GA-imprinted monolith was carried out as follows: a pre-polymerization mixture was prepared by mixing GA, 4-VP, nickel acetate, EDMA, DMSO, DMF, [BMIM]BF_4 and AIBN, as shown in Table 1. The pre-polymerization mixture was sonicated for 15 min and introduced into a stainless steel column (100 mm × 4.6 mm). The ends of the column were sealed and the column was submerged in a 60°C water bath for 18 or 24 h. After polymerization, the column was flushed with acetonitrile to remove any unreacted reagents. Thereafter, the resulting monolithic column was washed with a mixture of methanol and acetic acid (9:1, v/v) until no template molecules were detected in the extraction solvent. A non-imprinted column (NIP) was prepared similarly in absence of GA.

Chromatographic evaluation

High performance liquid chromatography was performed on an Agilent 1100 series chromatographic system consisting of a G1311A pump, a G131513 DAD detector, a Rheodyne 7225 injector with a 20 μL loop, and a Vertex VT4820 temperature controller. Data processing was carried out by a HPCORE workstation. The detection was performed at 271 nm with a flow rate of 0.5 mL/min. All of mobile phases were filtered through a 0.22 μm membrane from Millipore before use. Column void volume was measured by injecting 20 μL of acetone (0.1%, v/v) in a mobile

RSC Advances Accepted Manuscript

phase of acetonitrile–acetate buffer (pH 3.6)(70/30, v/v).

Retention factor (k) is calculated as $(t_R - t_0)/t_0$, where t_R is the retention time of the eluted substance and to the retention time of the void marker. Imprinting factor (IF) is calculated as IF = k_{MIP}/ k_{NIP}, where k_{MIP} is the retention factor of the template molecule eluted from the imprinted polymer and k_{NIP} is the retention factor of the template molecule eluted from the non-imprinted polymer.[27]

Frontal analysis

The binding capacities of the imprinted and non-imprinted monoliths were investigated by frontal chromatography method. The elution was monitored at 271 nm and the mobile phase was methanol with a flow-rate of 1.0 $mLmin^{-1}$. A series of different concentrations of GA (0.1, 0.15, 0.2, 0.3, 0.4, 0.5, 0.6 and 0.7 mmol L^{-1}), were prepared in mobile phase and loaded onto the imprinted monolithic columns at 25°C. The break-through curves were first generated and the retention time was obtained from the time at half-height of the break-through curve. The number of binding sites (L_t) and the dissociation constant (K_d) are calculated using the following equation: [30]

$$1/\{[A]_0(V-V_0)\} = K_d/([A]_0 L_t) + 1/L_t \quad (3)$$

where $[A]_0$ is the concentration of the analyte. V and V_0 are the elution volumes of the analyte and the void marker, respectively, which is calculated from the void time (acetone) and retention time of template multiplied by the flow rate. L_t and K_d can be calculated from the intercepts on the ordinate and the slope based on the plots of the $1/\{[A]_0(V-V_0)\}$ versus $1/[A]_0$.

RSC Advances Accepted Manuscript

Adsorption quantity of equilibrium in the frontal analysis, Q, is calculated by:[30]

$$Q = \frac{C(V_{equ} - V_0)}{V_a} \quad (4)$$

where C is sample concentration, V_{equ} is the volume when the adsorption is balanced, and V_a is stationary phase volume.

Acknowledgments

This work was supported by the High Technology Research and Development Program of Xinjiang (No. 201217149).

RSC Advances Accepted Manuscript

References

1 E. Saridakis, and N. E. Chayen, *Trends Biotechnol.*, 2013, **31**, 515.

2 Y. Ge, B. Butler, F. Mirza, S. Habib-Ullah, and D. Fei, *Macromol. Rapid Commun.*, 2013, **34**, 903.

3 B. Tóth, and G. Horvai, *Top Curr. Chem.*, 2012, **325**, 267.

4 A. Rahmani, A. H. Mohammadpour, A. Sahebnasagh, and S. A. Mohajeri, *Anal. Bioanal. Chem.*, 2014, **406**, 7729.

5 C. Zheng, Y. P. Huang, and Z. S. Liu, *Anal. Bioanal. Chem.*, 2013, **405**, 2147.

6 B. C. Iacob, E. Bodoki, and R. Oprean, *Electrophoresis*, 2014, **35**, 2722.

7 X. N. Wang, R. P. Liang, X. Y. Meng, and J. D. Qiu, *J. Chromatogr. A*, 2014, **1362**, 301.

8 X. Shen, L. Zhu, N. Wang, L. Ye, and H. Tang, *Chem. Commun.*, 2012, **48**, 788.

9 M.M. Moein, D. Jabbar, A. Colmsjö, and M. Abdel-Rehim, *J. Chromatogr. A*, 2014, **1366**, 15.

10 A. Tieppo, C. J. White, A. C. Paine, M. L. Voyles, M. K. McBride, and M. E. Byrne, *J. Control Release*, 2012, **157**, 391.

11 F. Puoci, G. Cirillo, M. Curcio, O.I. Parisi, F. Iemma, and N. Picci, *Expert Opin Drug Deliv.*, 2011, **8**, 1379.

12 G. Wulff, and J. Liu, *Acc. Chem. Res.*, 2012, **45**, 239.

13 A. Yarman, and F. W. Scheller, *Angew. Chem. Int. Ed. Engl.*, 2013, **52**, 11521.

14 M. P. Tiwari, and A. Prasad, *Anal. Chim. Acta*, 2015, **853**, 1.

15 Y. Fuchs, O. Soppera, and K. Haupt, *Anal. Chim. Acta*, 2012, **717**, 7.

RSC Advances Accepted Manuscript

16 C. Malitesta, E. Mazzotta, R.A. Picca, A. Poma, I. Chianella, and S.A. Piletsky, *Anal. Bioanal. Chem.*, 2012, **402**, 1827.

17 G. Wulff, *Angew. Chem. Int. Ed. Engl.*, 1995, **34**, 1812.

18 T. Kubo, K. Hosoy, M. Nomachi, N. Tanaka, and K. Kaya, *Anal. Bioanal. Chem.*, 2005, **382**, 1698.

19 J. Cao, X. Zhang, X. He, L. Chen, and Y. Zhang, *Chem. Asian. J.*, 2014, **9**, 526.

20 A. Pardo, L. Mespouille, P. Dubois, B. Blankert, and P. Duez, *Chem. Eur. J.*, 2014, **20**, 3500.

21 J.L. Urraca, M.C. Moreno-Bondi, A.J. Hall, and B. Sellergren, Anal. Chem., 2007, 79, 695.

22 P. Manesiotis, Q. Osmani, and P. McLoughlin, *J. Mater. Chem.*, 2012, **22**, 11201.

23 J. Matsui, S. Goji, T. Murashima, D. Miyoshi, S. Komai, A. Shigeyasu, T. Kushida, T. Miyazawa, T. Yamada, K. Tamaki, and N. Sugimoto, *Anal. Chem.*, 2007, **79**, 1749.

24 X.-X. Li, L.-H. Bai, H. Wang, J. Wang, Y.-P. Huang, and Z.-S. Liu, *J. Chromatogr. A*, 2012, **1251**, 141.

25 L. N. Mu, X. H. Wang, L. Zhao, Y.P. Huang, and Z.S. Liu, *J. Chromatogr. A*, 2011, **1218**, 9236.

26 S. J Li, C. Liao, W. Li, Y. Chen, and X. Hao, *Macromol. Biosci.*, 2007, **7**, 1112.

27 L. Zhao, L. Ban, Q.W. Zhang, Y. P. Huang, and Z. S. Liu, *J. Chromatogr. A*, 2011, **1218**, 9071.

28 G. Qu, S. Zheng, Y. Liu, W. Xie, A. Wu, and D. Zhang, *J. Chromatogr. B,* 2009,

RSC Advances Accepted Manuscript

877, 3187.

29 D.-D. Zhong, Y.-P. Huang, X.-L. Xin, Z.-S. Liu, and H. A. Aisa, *J. Chromatogr. B*, 2013, **934**, 109.

30 X. Sun, C.-Y. Zhao, X.-H. Wang, Y.-P. Huang, and Z.-S. Liu, *Anal. Bioanal. Chem.*, 2014, **406**, 5359.

31 K.S.W. Sing, *Pure Appl. Chem.*, 1982, **54**, 2201.

32 Y. P. Huang, S. J. Zhang, X. Wu, Q. W. Zhang, and Z. S. Liu, *Chromatographia*, 2009, **70**, 691.

33 H.S. Andersson, J.G. Karlsson, S.A. Piletsky, A.-C. Koch-Schmidt, K. Mosbach, and I. A. Nicholls, *J. Chromatogr. A*, 1999, **848**, 39.

34 G. Wulff, *Chem. Rev.*, 2002, **102**, 1.

35 A.G. Mayes, and K. Mosbach, *Anal. Chem.*, 1996, **68**, 3769.

36 B. Sellergren, and K.J. Shea, *J. Chromatogr. A*, 1993, **635**, 31.

37 B. Sellergren, *J. Chromatogr. A*, 2001, **906**, 227.

38 A. M. Rampey, R. J. Umpleby II, G. T. Rushton, J. C. Iseman, R. N. Shah, and K. D. Shimizu, *Anal. Chem.*, 2004, **76**, 1123.

RSC Advances Accepted Manuscript

Legends

Fig. 1. Structures of GA and analogues tested.

Fig. 2. Selectivity evaluation of the MIPs, NIPs. C11, C15, C5: MIPs; C12, C16, C6: NIPs. Mobile phase: acetonitrile-NaAc/HAc buffer (50 $mmolL^{-1}$, pH 5.0), 70/30 (v/v); detection wave length: 271 nm; flow rate: 0.5 $mLmin^{-1}$; injection: 20 μL; temperature: 25 ºC.

Fig. 3 Schematic representation of the preparation of OEG-based MIP by use of metal ions as pivot, and of molecular recognition by the MIP.

Fig. 4. Scanning electron micrographs of the following samples: (a) Ni^{2+}-mediated OEG MIP (C11); (b) Ni^{2+}-mediated OEG-free MIP (C15); (c) Ni^{2+}-free OEG MIP (C5).

Fig. 5. (a) Nitrogen adsorption-desorption isotherms for Ni^{2+}-mediated OEG MIP, Ni^{2+}-free OEG MIP and Ni^{2+}-mediated OEG-free MIP at 77 K; (b) Differential pore size distribution curves of Ni^{2+}-mediated OEG MIP, Ni^{2+}-free OEG MIP and Ni^{2+}-mediated OEG-free MIP.

Fig. 6. Retention factor and imprinting factor on Ni^{2+}-mediated OEG MIP prepared with different ratio of OEG to 4-VP. Mobile phase, acetonitrile/acetate buffer (50 mmol L^{-1}, pH 5.0) (70/30, v/v); flow rate, 0.5 mL min^{-1}; detection wavelength, 271 nm; injected volume, 20 μL; temperature, 25 ºC.

Fig. 7. Retention factor and imprinting factor on Ni^{2+}-mediated OEG MIP prepared with different levels of EDMA. Mobile phase, acetonitrile/acetate buffer (50 mmol L^{-1}, pH 5.0) (70/30, v/v); flow rate, 0.5 mL min^{-1}; detection wavelength, 271 nm;

RSC Advances Accepted Manuscript

injected volume, 20 μL; temperature, 25 ºC.

Fig. 8. Influence of the pH value of mobile phase on the retention factors of GA and imprinting factor on Ni^{2+}-mediated OEG MIP (C11); (b) Ni^{2+}-mediated OEG-free MIP (C15); (c) Ni^{2+}-free OEG MIP (C5) and respective NIPs. HPLC conditions: column temperature, 25 ºC; mobile phase, acetonitrile/acetate buffer (50 mmol L^{-1}) (70/30, v/v); flow rate, 0.5 mL min^{-1}; detection wavelength, 271 nm; injected volume, 20 μL.

Fig. 9. Influence of organic phase composition on the retention factors of GA and imprinting factor on Ni^{2+}-mediated OEG MIP (C11); (b) Ni^{2+}-mediated OEG-free MIP (C15); (c) Ni^{2+}-free OEG MIP (C5) and respective NIPs. HPLC conditions: column temperature, 25 ºC; mobile phase, acetonitrile/acetate buffer (50 mmol L^{-1}, pH 3.6); flow rate, 0.5 mL min^{-1}; detection wavelength, 271 nm; injected volume, 20 μL.

Fig. 10. Freundlich analysis for Ni^{2+}-mediated OEG MIP (C11); Ni^{2+}-mediated OEG-free MIP (C15) and Ni^{2+}-free OEG MIP (C5).

RSC Advances Accepted Manuscript

508 **Table 1** Preparation protocol for OEG MIP monoliths

Column	GA (mg)	$Ni(Ac)_2$ (mg)	4-VP (μL)	OEG (μL)	EDMA (μL)	DMF (μL)	DMSO (μL)	$[BMIM]BF_4$ (μL)	Time (h)
C1-MIP	17.01	24.88	64	343	453	240	1200	2468	18
C2-MIP	17.01	24.88	64	343	453	240	1200	2468	24
C3-MIP	17.01	24.88	64	343	453	240	1200	2468	24
C4-NIP	---	24.88	64	343	453	240	1200	2468	24
C5-MIP	17.01	---	64	343	453	240	1200	2468	24
C6-NIP	---	---	64	343	453	240	1200	2468	24
C7-MIP	17.01	12.44	64	343	453	240	1200	2468	24
C8-NIP	---	12.44	64	343	453	240	1200	2468	24
C9-MIP	17.01	24.88	64	343	339	240	1200	2468	24
C10-NIP	---	24.88	64	343	339	240	1200	2468	24
11-MIP	17.01	24.88	64	343	630	240	1200	2468	18
C12-NIP	---	24.88	64	343	630	240	1200	2468	18
C13-MIP	17.01	24.88	64	343	1018	240	1200	2468	18
C14-NIP	---	24.88	64	343	1018	240	1200	2468	18
C15-MIP	17.01	24.88	64	---	630	240	1200	2468	18
C16-NIP	---	24.88	64	---	630	240	1200	2468	18
C17-MIP	17.01	24.88	64	171	630	240	1200	2468	18
C18-NIP	---	24.88	64	171	630	240	1200	2468	18
C19-MIP	17.01	24.88	64	511	630	240	1200	2468	18
C20-NIP	---	24.88	64	511	630	240	1200	2468	18
C21-MIP	17.01	24.88	64	426	630	240	1200	2468	18
C22-NIP	---	24.88	64	426	630	240	1200	2468	18
C23-MIP	17.01	24.88	64	255	630	240	1200	2468	18
C24-NIP	---	24.88	64	255	630	240	1200	2468	18

RSC Advances Accepted Manuscript

509

510 **Table 2** Adsorption parameters of different MIPs

511

Column	Freundlich fitting			Scatchard-Rosenthal analysis		
	n	K_f (mmol/L)	R^2	K_d (mol/g)	Q (μmol/g)	R^2
C11-MIP	0.87	0.452	0.998	$K_{d\,1}=9.26\times10^{-4}$	Q_1 =32.2	0.993
				$K_{d\,2}=5.03\times10^{-3}$	Q_2 =114.5	0.975
C15-MIP	0.65	0.0028	0.990	$K_{d\,1}=5.49\times10^{-3}$	Q_1 =50.8	0.994
				$K_{d\,2}=7.14\times10^{-3}$	Q_2 =65.0	0.990
C5-MIP	0.67	0.793	0.988	$K_{d\,1}=1.24\times10^{-3}$	Q_1 =64.8	0.996
				$K_{d\,2}=4.63\times10^{-3}$	Q_2 =208.6	0.999

RSC Advances Accepted Manuscript

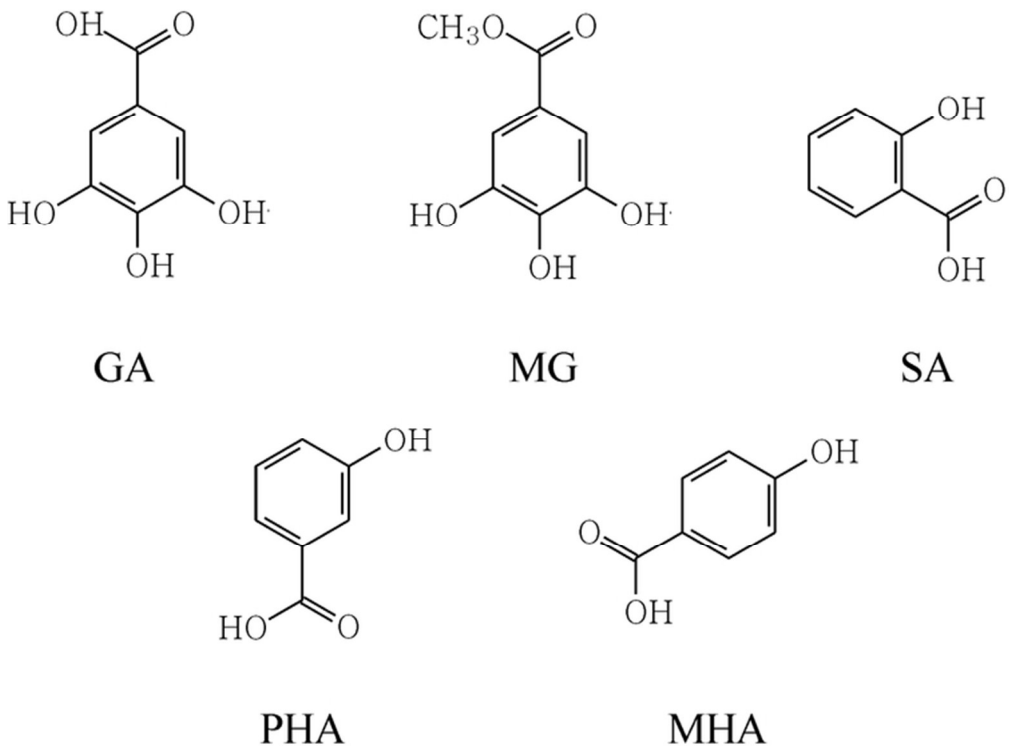

Fig. 1. Structures of GA and analogues tested.
31x23mm (600 x 600 DPI)

RSC Advances Accepted Manuscript

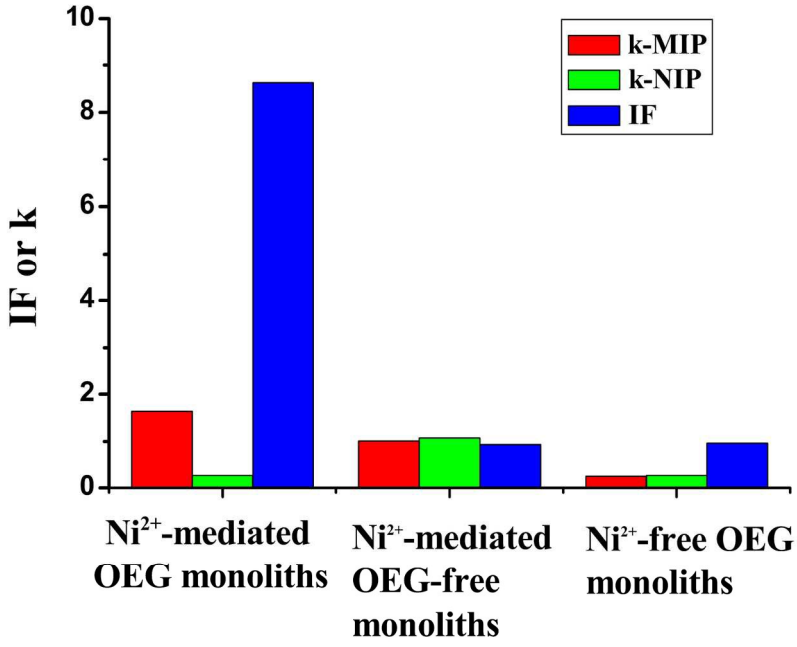

Fig. 2. Selectivity evaluation of the MIPs, NIPs. C11, C15, C5: MIPs; C12, C16, C6: NIPs. Mobile phase: acetonitrile-NaAc/HAc buffer (50 mmolL-1, pH 5.0), 70/30 (v/v); detection wave length: 271 nm; flow rate: 0.5 mLmin-1; injection: 20 μL; temperature: 25 ºC.
89x63mm (600 x 600 DPI)

RSC Advances Accepted Manuscript

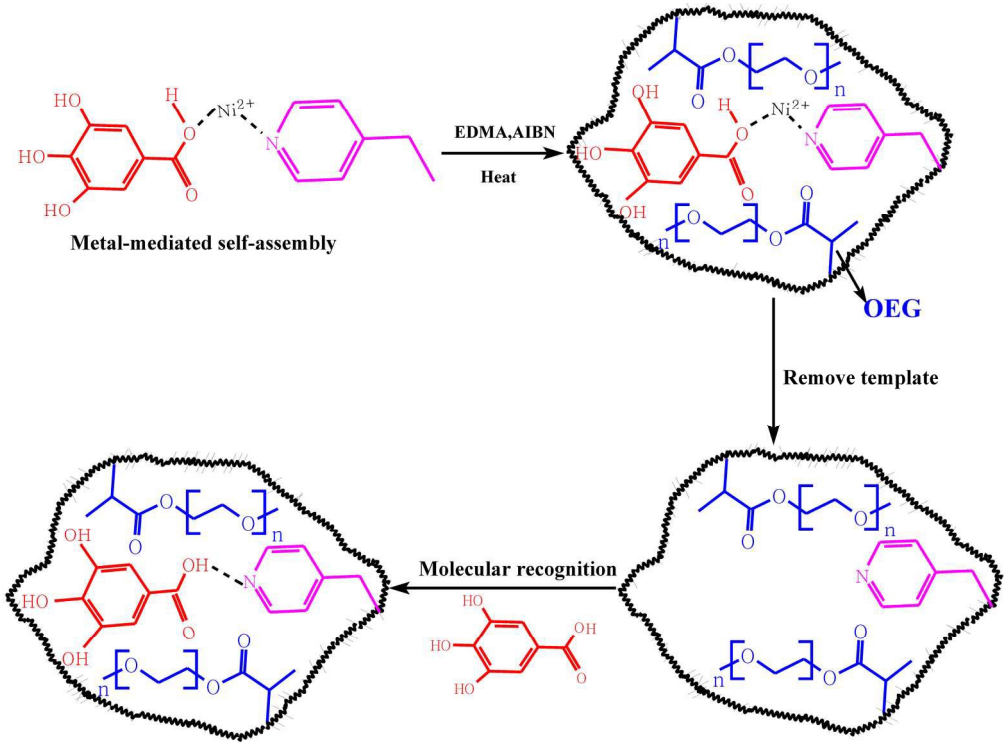

Fig. 3 Schematic representation of the preparation of OEG-based MIP by use of metal ions as pivot, and of molecular recognition by the MIP.
93x69mm (600 x 600 DPI)

RSC Advances Accepted Manuscript

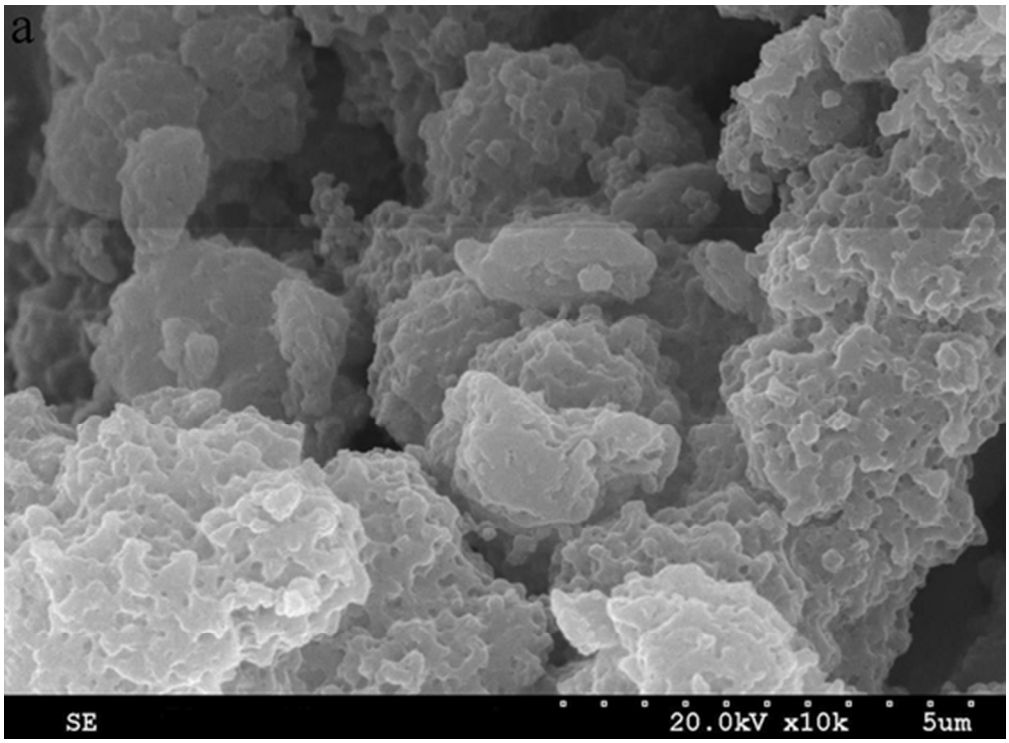

Fig. 4(a). Scanning electron micrographs of the following samples: Ni2+-mediated OEG MIP (C11
23x17mm (600 x 600 DPI)

RSC Advances Accepted Manuscript

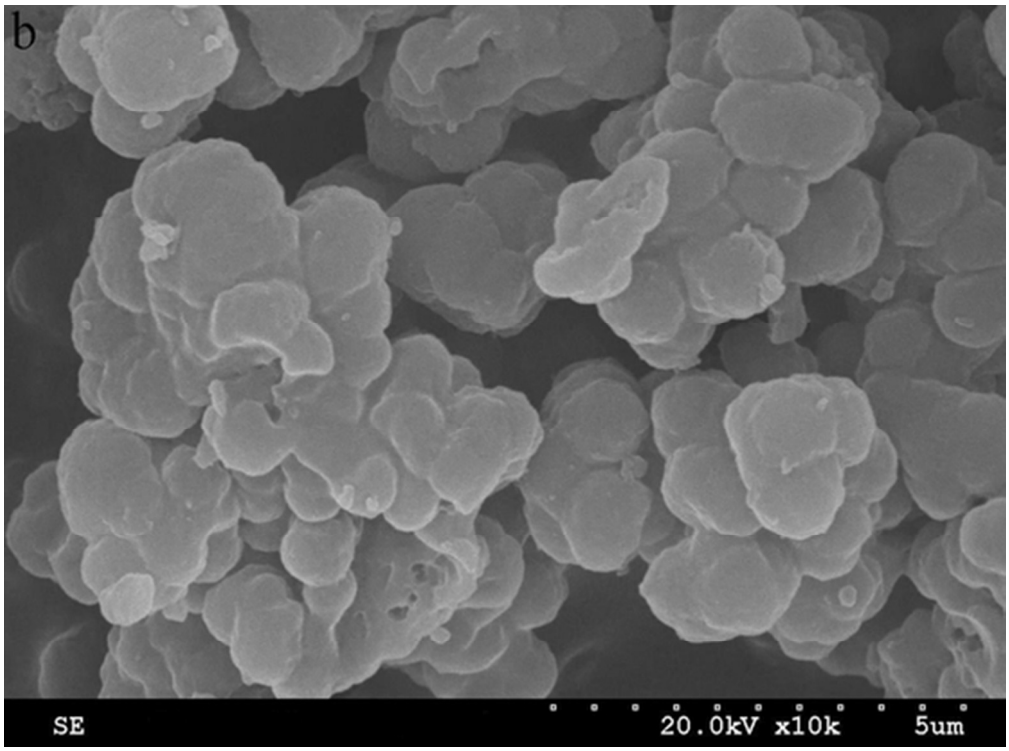

Fig. 4(b). Scanning electron micrographs of the following samples: Ni2+-mediated OEG-free MIP (C15)
23x17mm (600 x 600 DPI)

RSC Advances Accepted Manuscript

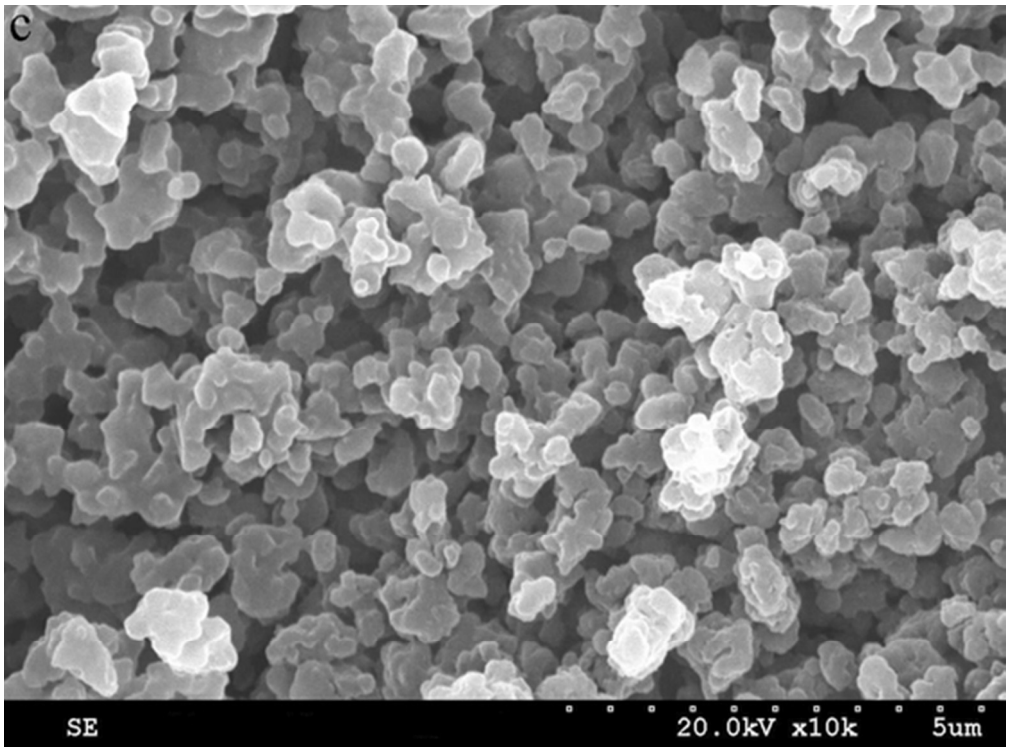

Fig. 3(c). Scanning electron micrographs of the following samples: Ni2+-free OEG MIP (C5)
23x17mm (600 x 600 DPI)

RSC Advances Accepted Manuscript

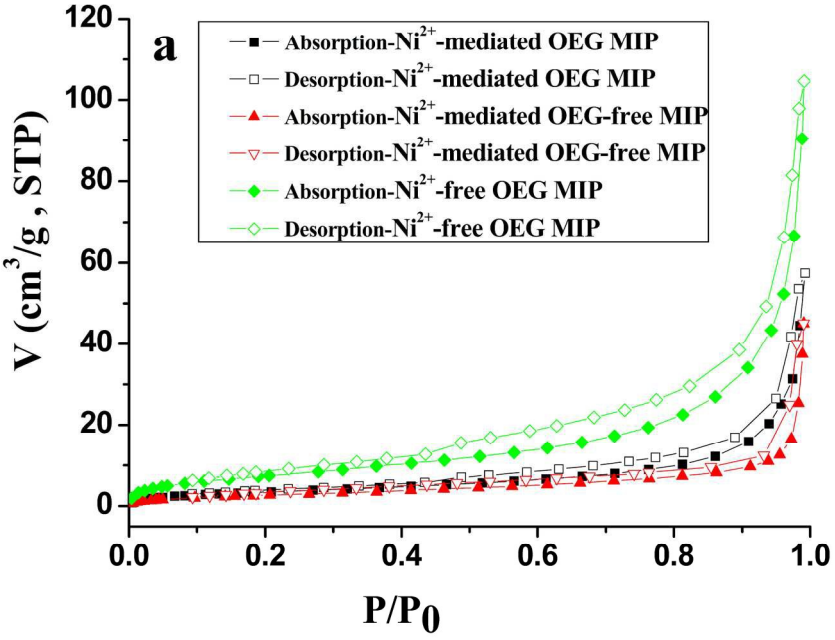

Fig. 5(a) Nitrogen adsorption-desorption isotherms for Ni2+-mediated OEG MIP, Ni2+-free OEG MIP and Ni2+-mediated OEG-free MIP at 77 K
89x63mm (600 x 600 DPI)

RSC Advances Accepted Manuscript

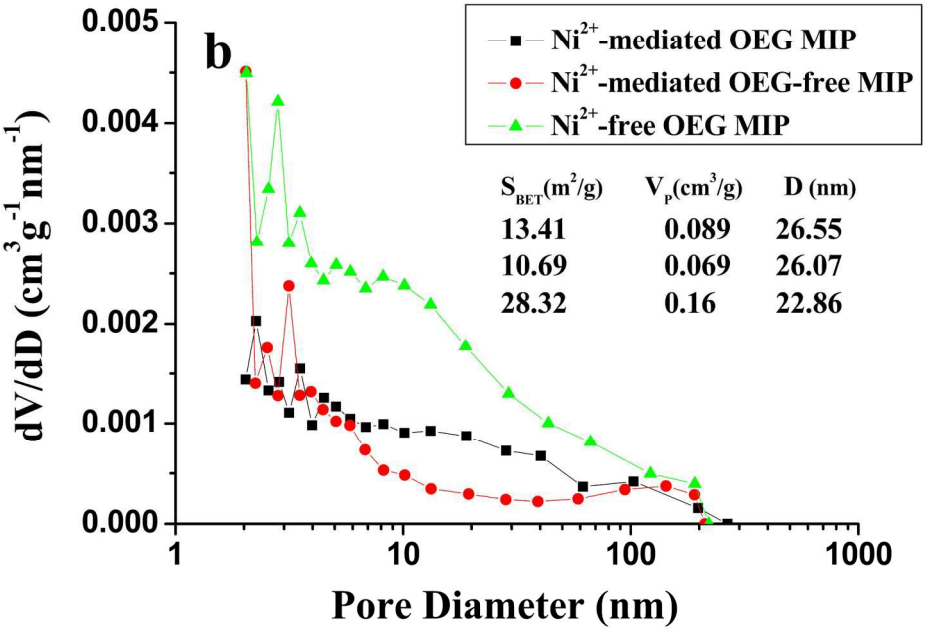

Fig. 5(b) Differential pore size distribution curves of Ni2+-mediated OEG MIP, Ni2+-free OEG MIP and Ni2+-mediated OEG-free MIP.
88x61mm (600 x 600 DPI)

RSC Advances Accepted Manuscript

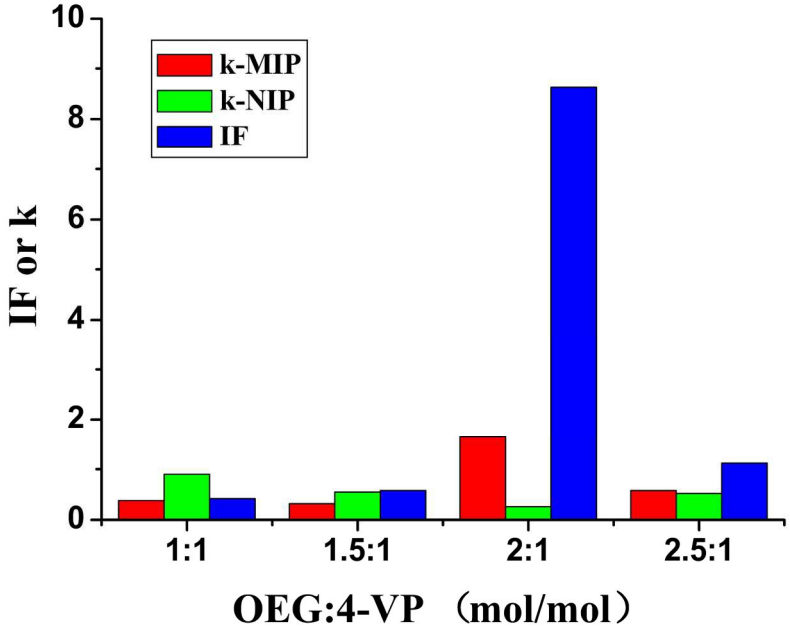

Fig. 6. Retention factor and imprinting factor on Ni2+-mediated OEG MIP prepared with different ratio of OEG to 4-VP. Mobile phase, acetonitrile/acetate buffer (50 mmol L−1, pH 5.0) (70/30, v/v); flow rate, 0.5 mL min−1; detection wavelength, 271 nm; injected volume, 20 μL; temperature, 25 ºC.
88x61mm (600 x 600 DPI)

RSC Advances Accepted Manuscript

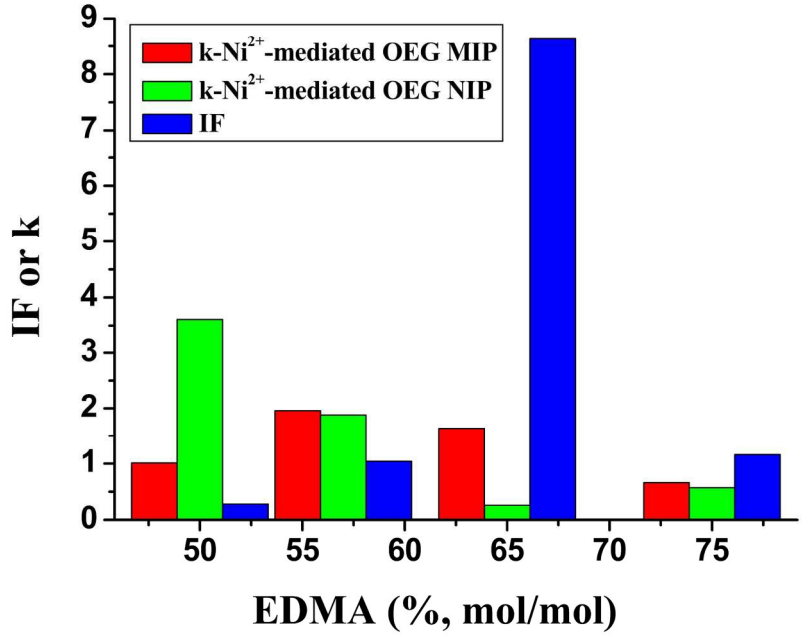

Fig. 7. Retention factor and imprinting factor on the Ni2+-mediated OEG MIP prepared with different levels of EDMA. Mobile phase, acetonitrile/acetate buffer (50 mmol L−1, pH 5.0) (70/30, v/v); flow rate, 0.5 mL min−1; detection wavelength, 271 nm; injected volume, 20 μL; temperature, 25 ºC.
88x61mm (600 x 600 DPI)

RSC Advances Accepted Manuscript

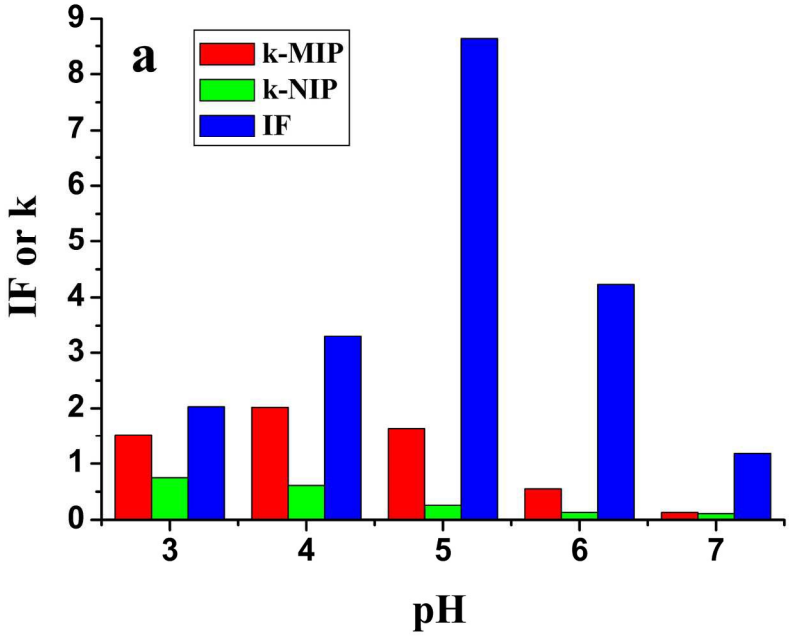

Fig. 8(a). Influence of the pH value of mobile phase on the retention factors of GA and imprinting factor on the Ni2+-mediated OEG MIP (C11) and respective NIPs. HPLC conditions: column temperature, 25 ºC; mobile phase, acetonitrile/acetate buffer (50 mmol L−1) (70/30, v/v); flow rate, 0.5 mL min-1; detection wavelength, 271 nm; injected volume, 20 µL.
88x61mm (600 x 600 DPI)

RSC Advances Accepted Manuscript

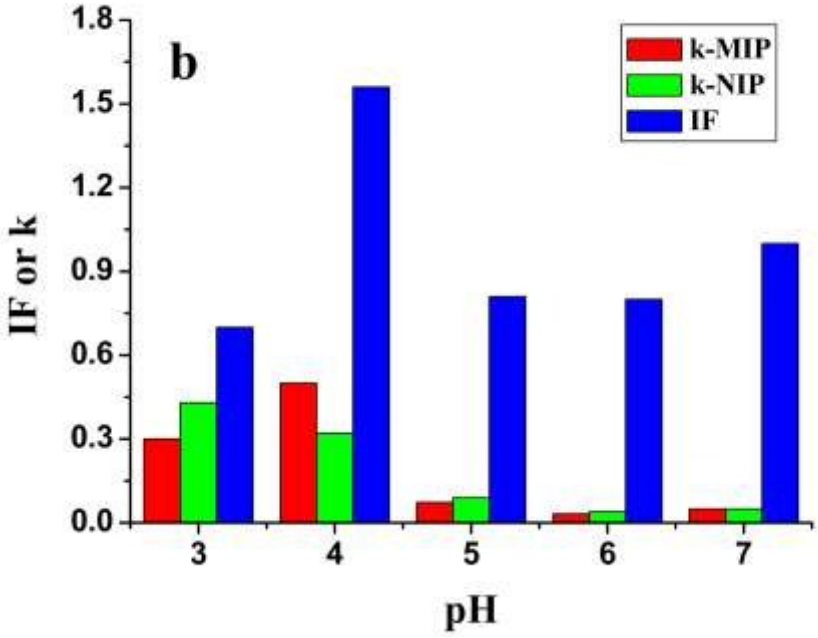

Fig. 8(b). Influence of the pH value of mobile phase on the retention factors of GA and imprinting factor on the Ni2+-mediated OEG-free MIP (C15) and NIPs. HPLC conditions: column temperature, 25 ºC; mobile phase, acetonitrile/acetate buffer (50 mmol L−1) (70/30, v/v); flow rate, 0.5 mL min-1; detection wavelength, 271 nm; injected volume, 20 μL.
88x61mm (600 x 600 DPI)

RSC Advances Accepted Manuscript

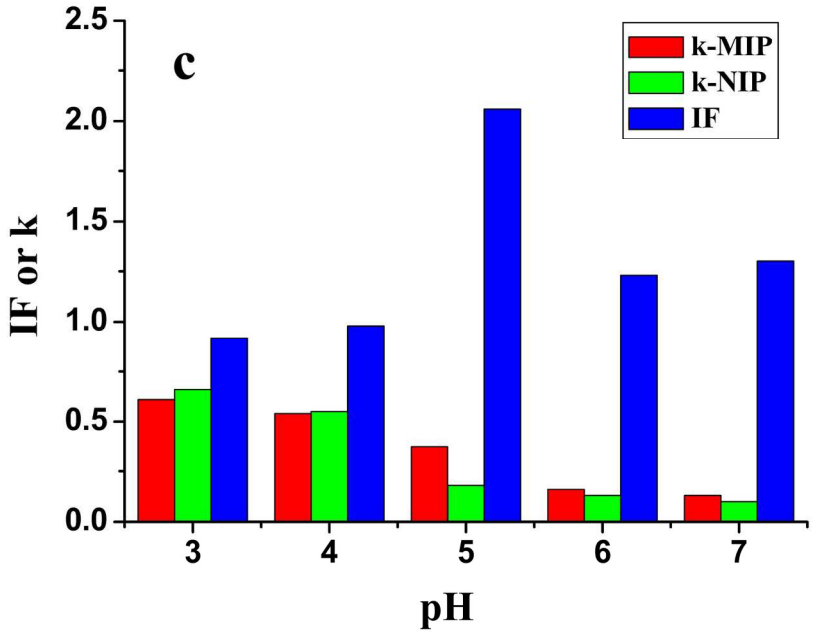

Fig. 8(c). Influence of the pH value of mobile phase on the retention factors of GA and imprinting factor on the Ni2+-free OEG MIP (C5) and NIPs. HPLC conditions: column temperature, 25 ºC; mobile phase, acetonitrile/acetate buffer (50 mmol L−1) (70/30, v/v); flow rate, 0.5 mL min-1; detection wavelength, 271 nm; injected volume, 20 μL.
88x61mm (600 x 600 DPI)

RSC Advances Accepted Manuscript

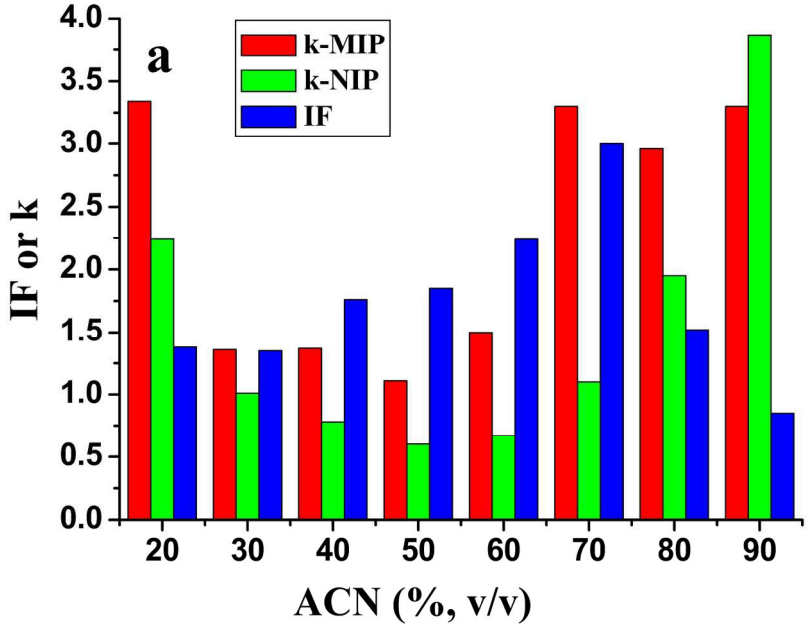

Fig. 9(a). Influence of organic phase composition on the retention factors of GA and imprinting factor on the Ni2+-mediated OEG MIP (C11) and NIPs. HPLC conditions: column temperature, 25 ºC; mobile phase, acetonitrile/acetate buffer (50 mmol L-1, pH 3.6); flow rate, 0.5 mL min-1; detection wavelength, 271 nm; injected volume, 20 µL.
88x61mm (600 x 600 DPI)

RSC Advances Accepted Manuscript

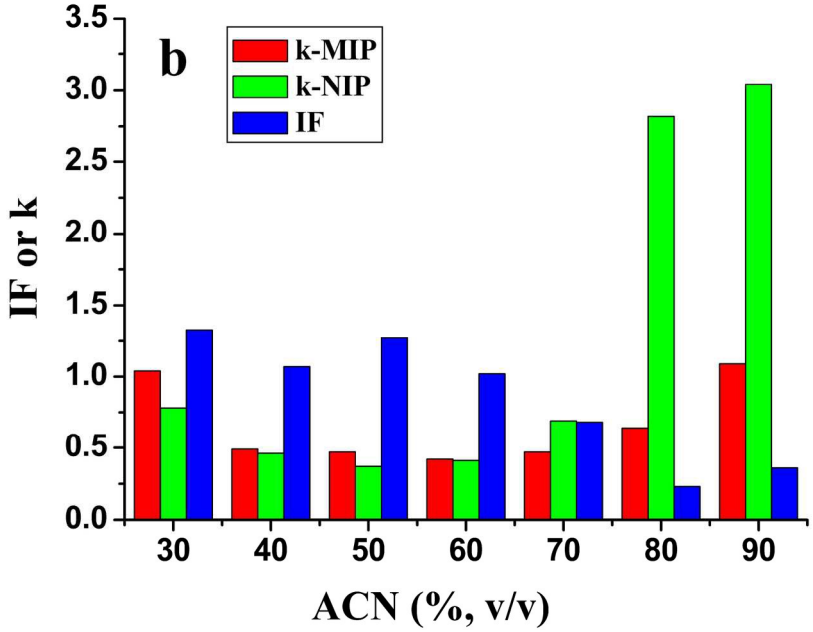

Fig. 9b. Influence of organic phase composition on the retention factors of GA and imprinting factor on Ni2+-mediated OEG-free MIP (C15) and NIP. HPLC conditions: column temperature, 25 ºC; mobile phase, acetonitrile/acetate buffer (50 mmol L-1, pH 3.6); flow rate, 0.5 mL min-1; detection wavelength, 271 nm; injected volume, 20 µL.
88x61mm (600 x 600 DPI)

RSC Advances Accepted Manuscript

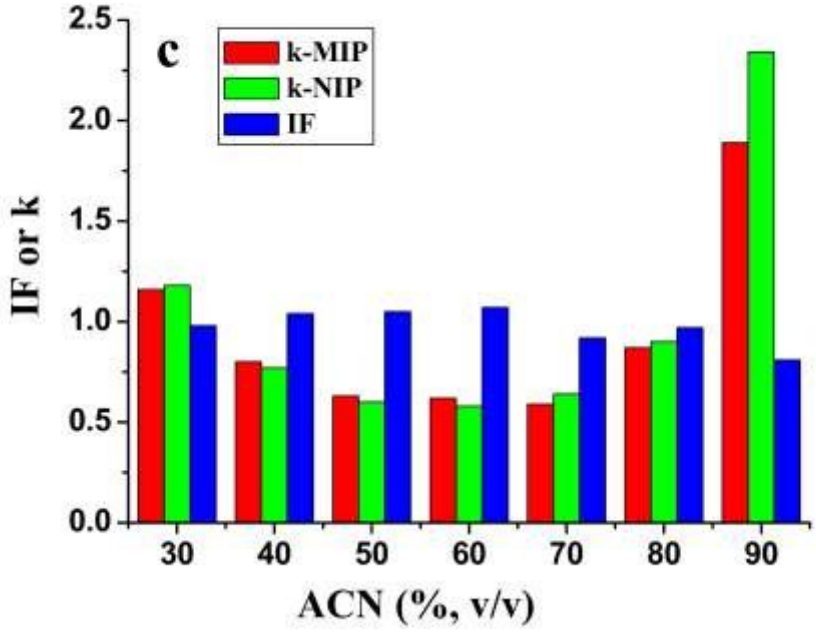

Fig. 9c. Influence of organic phase composition on the retention factors of GA and imprinting factor on Ni2+-free OEG MIP (C5) and NIP. HPLC conditions: column temperature, 25 ºC; mobile phase, acetonitrile/acetate buffer (50 mmol L-1, pH 3.6); flow rate, 0.5 mL min-1; detection wavelength, 271 nm; injected volume, 20 µL.
88x61mm (600 x 600 DPI)

RSC Advances Accepted Manuscript

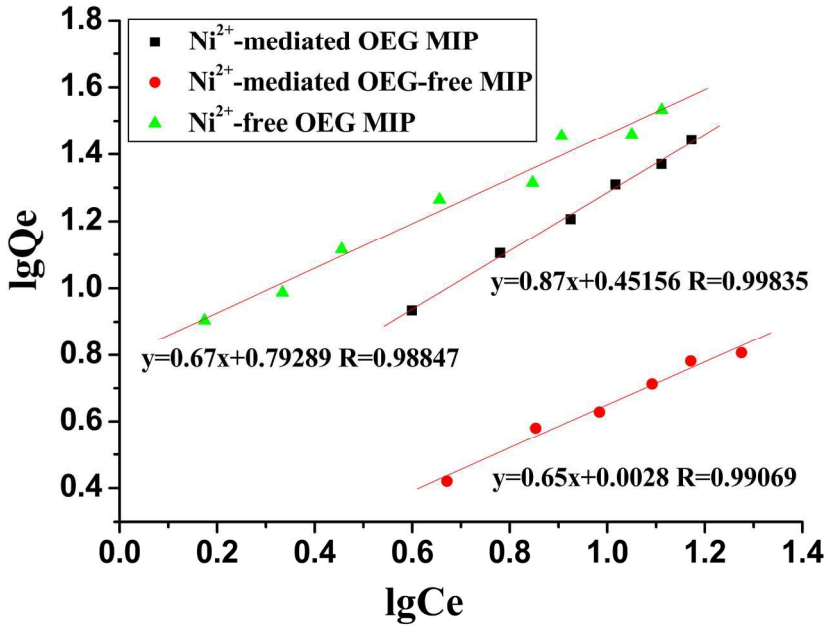

Fig. 9. Freundlich analysis for the Ni2+-mediated OEG MIP (C11); Ni2+-mediated OEG-free MIP (C15) and Ni2+-free OEG MIP (C5).
88x61mm (600 x 600 DPI)

RSC Advances Accepted Manuscript